**Showcasing research led by Prof. Nguyen T. K. Thanh's group at University College London, UK. This work was carried out with contributions from colleagues at the Laboratory of Coordination Chemistry (LCC-CNRS, Toulouse, France), the University of Vigo, Spain, and the Aristotle University of Thessaloniki, Greece.**

A parametric study on CoFe-based ferrite and alloy nanoparticle synthesis

The exploratory systematic synthesis of cobalt ferrite and FeCo alloy nanoparticles *via* colloidal chemical routes is presented in this work. A range of parameters were investigated so as to unravel their effect on properties of the resulting nanostructures such as composition, size, shape, magnetism and heating efficiency.

Image reproduced by permission of Nguyen T. K. Thanh and Antonios Makridis from *Nanoscale*, 2025, **17**, 17110.

ROYAL SOCIETY OF CHEMISTRY

rsc.li/nanoscale

Check for updates

A parametric study on CoFe-based ferrite and alloy nanoparticle synthesis†
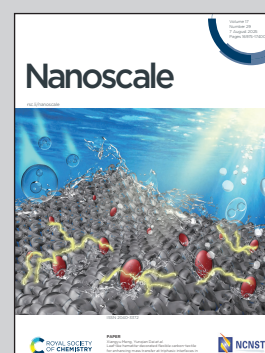
Andreas Sergides,[a,b] Catherine Amiens, [ID][c] Sergio Gómez-Graña,[d]
Antonios Makridis, [ID][e,f] Liudmyla Storozhuk, [ID][a,b] Stefanos Mourdikoudis [ID] *[a,b,d]
and Nguyen Thi Kim Thanh [ID] *[a,b]

Magnetic nanoparticles (MNPs) have received great attention over the last two decades thanks to their potential uses in various application fields such as high-density recording media, magnetic separation and biomedicine. In this work we focus on the exploratory synthesis of cobalt ferrite and iron–cobalt NPs through thermal decomposition wet-chemical pathways. Several parameters were examined in order to elucidate their impact on the composition, morphology and magnetic behaviour of the produced nanomaterials. A range of metallic precursor types is first investigated, with a subsequent focus on the case of acetylacetonate salts. In addition, the reduction of $CoFe_2O_4$ to FeCo by employing a salt-matrix annealing stage is explored. Polyol and H_2-mediated methods are utilized to prepare FeCo alloy NPs in a direct manner. Multi-core nanostructures were also synthesized, and they are very promising for magnetic resonance imaging (MRI) and magnetic hyperthermia (MH) applications. The post-synthesis thermal treatment helped to convert ferrites to an iron–cobalt alloy, with the expense of significant particle size increase and aggregation. Alloy particles formed in a one-pot synthesis by polyol routes had a >100 nm size and hexagonal shape, while hydrogen-assisted reduction led to monodisperse ~30 nm NPs with remarkable MH properties.

1. Introduction

The unique characteristics of MNPs arise from the fact that these magnets demonstrate in the nanoscale different properties compared to their bulk counterparts, due to the higher surface-to-volume ratio. MNPs are suitable for environmental and theranostic applications, among other fields. For instance, they can combine diagnosis MRI and therapy (MH for cancer treatment). Among various NP types, magnetite (Fe_3O_4) and maghemite (γ-Fe_2O_3) have been extensively studied over the last few decades. Research in the field is ongoing with other promising materials gaining increasing attention, such as doped-ferrites ($M_xFe_{3-x}O_4$, M: cobalt,[1,2] zinc,[3,4] manganese,[5,6] and magnesium[7,8]), zerovalent iron[9,10] and alloys[11,12] (Fe–Co,[13,14] Fe–Pt,[15,16] Ni–Co[17] and others).

Cobalt ferrite (general formula: $Co_xFe_{3-x}O_4$) exhibits an inverse spinel structure in which all Co^{2+} ions are located in octahedral sites (B sites) and Fe^{3+} ions are equally distributed between tetrahedral (A sites) and B sites. Typically, ferrites have a superparamagnetic size limit of 10 nm. However, the critical size of $CoFe_2O_4$ for superparamagnetic behavior is below 10 nm (around 5 nm), due to its large magnetocrystalline anisotropy.[18] In addition, the superparamagnetic behavior of such NPs is compositionally dependent. Fantechi *et al.* studied the influence of cobalt doping on Fe_3O_4. When $x = 0.4$–0.6, the as-prepared 8 nm NPs are superparamagnetic at temperatures higher than room temperature.[19] FeCo alloys are soft magnetic materials demonstrating a body-centered cubic (bcc) structure. They exhibit the highest M_s among any other magnetic materials (bulk M_s: 240–245 A m^2 kg^{-1}, while bulk M_s of Fe, Co, Fe_3O_4, γ-Fe_2O_3 and $CoFe_2O_4$ are 218, 161, 92, 80 and 80–85 A m^2 kg^{-1} respectively). Moreover, Co is the only element that increases the M_s when alloyed with Fe (55–65% Fe). Of course, variations in the composition and particularly in the Fe/Co ratio in ferrite and alloy nanostructures cause an alteration of their magnetic properties, as in the bulk.[20] These remarkable properties of FeCo NPs in the superparamagnetic

[a]Biophysics Group, Department of Physics and Astronomy, University College London (UCL), London, WC1E 6BT, UK. E-mail: ntk.thanh@ucl.ac.uk, s.mourdikoudis@ucl.ac.uk

[b]UCL Healthcare Biomagnetics and Nanomaterials Laboratories, 21 Albemarle Street, London, W1S 4BS, UK

[c]Université de Toulouse, CNRS, LCC, 205 Route de Narbonne, BP 44099, F-31077 Toulouse Cedex 4, France

[d]CINBIO, Universidade de Vigo, Materials Chemistry and Physics Group, Department of Physical Chemistry, Campus Universitario Lagoas Marcosende, 36310 Vigo, Spain

[e]Department of Condensed Matter and Materials Physics, Aristotle University of Thessaloniki, 54124 Thessaloniki, Greece

[f]Laboratory of Magnetic Nanostructure Characterization, Technology & Applications (MagnaCharta), Centre for Interdisciplinary Research and Innovation, Balkan Centre, Building B, 10th km Thessaloniki-Thermi Rd., 57001 Thessaloniki, Greece

regime (typically below 10 nm), in conjunction with their high heating efficiency,[21] ensure high potential for biomedical applications, especially MH. The synthesis of FeCo NPs though is quite tricky due to their poor chemical stability.

There is a vast number of methods used for the production of MNPs.[12,22,23,24–26] A comparison of the main synthetic approaches is presented in Table 1. Among these, co-precipitation and thermal decomposition are the most common synthetic routes, while the polyol method is frequently reported in the literature. Co-precipitation concerns the synthesis of MNPs from inorganic salts under alkaline conditions. It is a simple, fast and efficient chemical method and leads to one-step generation of water dispersible particles. By adjusting the pH, the particle size can be controlled relatively easily. However, the particles synthesized by this method suffer from poor crystallinity, which worsens the magnetic properties of the crystals. They also show a partial tendency for agglomeration. The thermal decomposition route has to do with the synthesis of MNPs *via* decomposition of organometallic precursors in the presence of surfactants (*e.g.* oleic acid, oleylamine and other usually hydrophobic molecules), in high boiling point organic solvents. This method results in the formation of highly crystalline and monodisperse NPs with very good control over size and shape. In the case of ferrite nanoparticles, Rinaldi and co-workers studied the role of different inert gases such as Ar and N_2 as well as molecular oxygen during thermal decomposition synthesis aiming to produce NPs with controlled oxidation, dimensions and magnetic properties.[27] Actually, the particles produced by thermal decomposition are often hydrophobic and hence further surface modification is needed to render the particles hydrophilic and suitable for biomedical applications. Other drawbacks include the use of high temperatures and organic solvents, which are not always easy to wash out and fully remove from the particle surface. The polyol method utilizes glycols (molecules with more than one hydroxyl group), such as ethylene, di-, tri-, and tetraethylene glycol, which serve as solvents, surfactants and mild reducing agents at the same time. The resulting nanocrystals are

hydrophilic, but polyol pathways are considered less effective when aiming to fine-tune the size and shape of NPs compared to thermal decomposition.

In the case of the synthesis of metallic (Fe, Co, and Ni) or bimetallic particles (FeCo, FePt, FeNi) some alternative synthetic approaches can be adopted. Fe and FeCo NPs were produced by thermolytic reduction of metal salts in high boiling point solvent, using strong reducing agents (such as lithium triethylborohydride[28] or hydrazine[29]). Desvaux *et al.* have reported the synthesis of FeCo NPs in sealed pressurized vessels (Fischer Porter bottles) in the presence of hydrogen gas,[13,30,31] while Thanh *et al.* studied the synthesis of magnetic alloys by thermal decomposition of bimetallic precursors, instead of using two individual precursors.[32] Finally, Wang *et al.* have published the synthesis of FeCo alloys by interfacial diffusion of Co/Fe core/shell NPs.[33] In this manuscript we study the synthesis of cobalt ferrite and iron–cobalt alloy NPs through thermal decomposition and polyol- and hydrogen-assisted routes. Following a well-designed variation of parameters such as precursors, surfactants and annealing conditions, useful insights on how the employed pathways affect the resulting NP features, such as composition, morphology and magnetic properties, were gathered. Even though we used colloidal chemistry for our synthetic approach, which is not an uncommon method for magnetic nanoparticles, the combination of the specific chemical protocols and pathways that we report here have not been published elsewhere. This study allowed us to produce NPs of interest for the biomedical field. The heating efficiency of selected alloy particles is then presented as a first step towards their use in MH applications.

2. Materials and methods

Unless otherwise stated, all reagents and solvents, apart from iron(III) oleate (Fe(ol)$_3$) and cobalt(II) oleate (Co(ol)$_2$), are commercially available and were used without further purification.

Table 1 Comparison of the main synthetic methods used to produce MNPs[25]

Method	Reaction and conditions	Reaction temperature (°C)	Reaction period	Size distribution	Shape control	Yield
Co-precipitation	Very simple, air/water	20–150	Minutes	Relatively narrow	Not good	High/scalable
Thermal decomposition	Complicated, inert atmosphere	100–350	Hours–days	Very narrow	Very good	High/scalable
Hydro- or solvothermal synthesis	Simple, high pressure/not always inert	150–220	Hours–days	Very narrow	Very good	High/scalable
Sol–gel and polyol method	Complicated, room temperature (RT) to higher T	25–200	Hours	Narrow	Good	Medium
Microemulsion	Complicated, not always inert	20–80	Hours	Narrow	Good	Low
Sonolysis or sonochemical method	Very simple, not always inert	20–50	Minutes	Narrow	Bad	Medium
Microwave-assisted synthesis	Very simple, not always inert	100–200	Minutes	Medium	Good	Medium
Biosynthesis	Complicated, not always inert	RT	Hours–days	Broad	Bad	Low
Electrochemical methods	Complicated, often in air	RT	Hours–days	Medium	Medium	Medium
Aerosol/vapour methods	Complicated, inert atmosphere	>100	Minutes–hours	Relatively narrow	Medium	High/scalable

Iron(III) acetylacetonate [Fe(acac)$_3$, 99+%], cobalt(II) acetyl-acetonate [Co(acac)$_2$, 99%], iron(II) chloride tetrahydrate [FeCl$_2$·4H$_2$O, 99+%], ethylene glycol (EG, 99+%), mesitylene (99+%) and oleylamine (OAm, 80–90%) were obtained from Acros Organics. Iron pentacarbonyl [Fe(CO)$_5$, 99.99%], ferrocene (98%), iron(III) chloride hexahydrate [FeCl$_3$·6H$_2$O, 99%], cobalt(II) acetate tetrahydrate [Co(CH$_3$COO)$_2$·4H$_2$O, 99.999%], 1,2-hexadecanediol (HDD, 90%), dioctyl ether (99%), oleic acid (OAc, 90%), sodium hydroxide (NaOH, pellets), sodium chloride (anhydrous, 99+%, free flowing), hexadecylamine (HDA, 98%) and 1,2-distearoyl-*sn*-glycero-3-phosphoethanolamine-*N*-[amino(polyethylene glycol)-2000] (DSPE-PEG) (ammonium salt) were purchased from Sigma-Aldrich. Co(N(Si(CH$_3$)$_3$)$_2$)$_2$, *i.e.* di-bis(trimethylsilyl)amido cobalt (II), was purchased from NanoMeps. Sodium oleate (97%), cobaltocene, hexane and absolute ethanol were bought from TCI, Alfa Aesar, Fluka, and Haymankimia, respectively. Tetrahydrofuran (THF, 99+%) was purchased from Carlo Erba. Methanol (≥99.8%) was bought from VWR, UK. The synthesis of Fe(ol)$_3$ and Co(ol)$_2$ was performed according to a common procedure reported in the literature.[34,35]

2.1 Synthesis by thermal decomposition

The synthesis of NPs was carried out using standard airless conditions (Schlenk line). A typical synthesis is based on the reductive thermal decomposition of a 3 mmol Fe-based precursor and a 2 mmol Co-based precursor in a mixture of surfactants (OAc and OAm, 20 mmol each) and 6 mmol HDD in 40 ml dioctyl ether, under a gas mixture of 95% N$_2$ + 5% H$_2$ (1200 ml min^{-1}) at 300 °C. The above mixture was degassed for 1.5 h at 75 °C. To ensure complete removal of oxygen and water, the mixture was then purged with N$_2$/H$_2$ gas for 45 min at 110 °C. Thereafter, the temperature was raised stepwise (5–7 °C min^{-1}) to 300 °C and the reaction mixture was refluxed for 1 h at that temperature (heat-up process). Then, the product was allowed to cool down to room temperature under gas flow. The as-prepared NPs were handled in air and washed 3–4 times with an hexane/ethanol mixture (1:2–1:3). The nanocrystals were isolated by magnetic separation each time. Finally, the product was dried by evaporating any residual solvents using gas flow (N$_2$/H$_2$).

2.2 Salt-matrix annealing procedure

A salt-matrix annealing procedure was adopted to reduce CoFe$_2$O$_4$ to FeCo NPs. NaCl powder was first ground with a mortar for 5 min to reduce powder grain size. The as-prepared CoFe$_2$O$_4$ NPs, after being washed and dried, were dispersed in hexane and mixed with NaCl powder, with a weight ratio of NPs to salt of 1:1000. The mixture was mechanically stirred and heated up to 65 °C until it is completely dry. Afterwards the mixture was annealed at 350–500 °C at a rate of ~10–15 °C min^{-1} under a mildly reducing gas (95% N$_2$ + 5% H$_2$) atmosphere (1200 ml min^{-1}) for 1–12 h. After annealing, the product was let to cool down to room temperature under gas flow, and washed 3 times with Milli-Q water and then 2 times with ethanol, followed by magnetic separation. The recovered NPs were dried by using a gas flow of N$_2$/H$_2$.

2.3 Polyol synthesis

2.24 mmol FeCl$_2$·4H$_2$O and 0.56 mmol Co(CH$_3$COO)$_2$·4H$_2$O were mixed with NaOH (10–40 mmol) and 40 ml EG. The mixture was then degassed with N$_2$/H$_2$ for 1.5 h at 110 °C. Afterwards, the temperature was raised stepwise (5–7 °C min^{-1}) to 200 °C and the reaction mixture was refluxed for 10 min^{-1} h^{-1} at this temperature. The product was allowed to cool down to room temperature under gas flow, and washed 5 times with methanol prior to magnetic separation.

2.4 Synthesis under a H$_2$ atmosphere

In the glovebox, 0.362 g (1.5 mmol) HDA and 0.19 g (0.25 mmol) Co(N(Si(CH$_3$)$_3$)$_2$)$_2$ were introduced in a Fisher–Porter bottle (FPB) followed by the addition of 0.424 g (1.5 mmol) OAc with the help of 10 ml mesitylene. Then, another 15 ml of mesitylene were added (25 ml in total), resulting in a clear purple solution. The FPB was removed from the glovebox and 0.13 ml (1 mmol) Fe(CO)$_5$ was added under airless conditions. The mixture was conditioned at 3 bar H$_2$ for 20 min and then heated at 150 °C by being placed in a pre-heated oil bath for 72 h under stirring (500 rpm). Mesitylene was dried by distillation over sodium before use (<5 ppm H$_2$O) and degassed with three freeze–pump–thaw cycles. After 3 d of reaction, the FPB was allowed to cool at room temperature and H$_2$ was evacuated. The magnetic NPs were isolated by magnetic separation, washed three times with dry (MBraun SPS-800 purification machine) and degassed THF in the glovebox, and dried under vacuum for 2 h.

2.5 Surface functionalization with a hydrophilic agent

FeCo alloys were functionalized with a hydrophilic phospholipid (DSPE-PEG) rendering them water dispersible. 10 mg of magnetic NPs were mixed with 4 ml THF in a vial and sonicated for 30 min. In a second vial, 20 mg of DSPE-PEG were also mixed with 4 ml THF in a vial and sonicated for 30 min. Then, the NP dispersion was added to the phospholipid solution with 0.2 ml aliquots under sonication. The resulting dispersion was further sonicated for 1.5–2 h and then agitated for 40–45 h. Afterwards, FeCo@DSPE-PEG NPs were precipitated with 30 ml hexane followed by centrifugation at 5000 rpm for 3 min. They were then dispersed in 6–7 ml THF with the help of sonication and vortex and then precipitated again with 30 ml hexane and centrifugation.

The NPs were dried in nitrogen flow and then dispersed in 15 ml distilled water, followed by 1 h sonication and agitation for 40–45 h. The excess phospholipid was removed through a centrifugal filter (Vivaspin 100 kDa MWCO). The mixture was centrifuged (4000 rpm, 2810g, swinging bucket rotor) until obtaining a concentrated (1–2 ml) dispersion (~30 min centrifugation for 10 ml), and the filtrate was discarded. Afterwards, the product was diluted with distilled water and centrifuged again. The concentration/dilution procedure was repeated 4–5 times to ensure complete removal of the unreacted ligand. The FeCo@DSPE-PEG NPs were collected from the filter with a few ml of water, sonicated for 30 min

and filtered (0.45 μm). An aliquot was taken for dynamic light scattering (DLS) measurement and the rest was freeze-dried.

2.6 Characterisation techniques

The size and morphology of the particles were examined by transmission electron microscopy (TEM) by depositing 20–30 μl of sample onto amorphous carbon coated copper grids. The TEM images were recorded on a JEOL 1200-EX electron microscope at a 120 kV accelerating voltage. We used Image-Pro plus software to determine the size of the particles (n = 200). HRTEM, high angle annular dark field imaging (HAADF) and scanning transmission electron microscopy (STEM) with EDX mapping were performed with a Titan G2 6300 equipped with a spherical aberration image corrector operating at 300 kV. Elemental mapping was carried out using STEM with a condenser aperture of 70 mm and a windowless silicon drift detector. The sample was tilted 15° towards the EDX detector for data acquisition. X-ray powder diffraction (XRD) patterns were obtained using an X'Pert Pro (PANalytical) diffractometer with a Co Kα X-ray source (λ = 1.7903 Å; 40 kV/40 mA), from 20 to 110°. The magnetic properties were investigated with a Quantum Design MPMS Superconducting Quantum Interference Device (SQUID) magnetometer with magnetic fields up to 7 T (70 kOe) at 300 K. Magnetization values are given at 7 T, and per kg of inorganic content in the sample as determined from thermogravimetric analysis (TGA). TGA was used to identify the inorganic percentage of the samples up to 600 °C (balance flow: 10 ml min^{-1}, sample flow (N$_2$): 25 ml min^{-1}, heating rate: 10 °C min^{-1}). Dysprosium oxide calibration curves were employed to correct the SQUID data (R software). A Varian 720 inductively coupled plasma atomic emission (ICP-AES) spectrometer was utilized to determine the Fe/Co ratios of several samples. For this purpose, powder samples were dissolved in concentrated HNO$_3$ at 60 °C. After that, the solutions were diluted with deionized water to obtain a 2% nitric acid solution for element quantification. X'Pert High Score plus software was utilized to analyze the XRD patterns. The heating abilities of the particles in an alternating magnetic field were assessed with a calorimetric analyzer (G2 driver D5 series, nB nanoScale Biomagnetics) at a frequency (f) of 488 kHz and a field strength (H) of 308 Oe (=24.5 kA m^{-1}), which are in the accepted range for measurement conditions. The temperature was recorded using a GaAs-based fiber optic probe inserted in a vial containing approximately 1 ml of the NP dispersion. A sealed glass (Dewar flask at <0.1 Pa) ensured the thermal insulation of the vial with the sample, helping it become a pseudoadiabatic system. The specific absorption rate (SAR) of the particles, the $\Delta T/\Delta t$ and the intrinsic loss power (ILP) values were determined as reported in our previous work.[36]

3. Results and discussion

Our initial objective was to perform the synthesis of NPs using various precursor types while keeping all other parameters constant, in order to investigate how different precursors affect the composition, morphology, size and magnetic properties of the nanocrystals. Afterwards we focused on Fe(acac)$_3$ and Co(acac)$_2$ precursors and explored how the surfactants, solvent and reaction time influence the NP characteristics described above. Furthermore, we examined the reduction of CoFe$_2$O$_4$ to FeCo *via* a salt-matrix annealing procedure. Apart from the thermal decomposition route, the synthesis of FeCo NPs *via* polyol or H$_2$-assisted methods was also investigated.

3.1. Thermal decomposition – different precursor pairs

The decomposition of iron and cobalt acetylacetonate occurs at similar temperatures (170–190 °C).[37] The decomposition of the precursors initiates the nucleation process, followed by the growth of nanocrystals. In fact, we have used a relative excess (2/1) of iron in respect to cobalt precursors under our synthetic conditions, and this occurred for two reasons: (i) the different electronegativities between the two metals imply distinct reactivities, with notably distinct reduction patterns and (ii) as mentioned in the Introduction, iron–cobalt alloys that are slightly Fe-rich are the ones with the highest magnetization.[20,30] The sample code names that follow denote the precursor pairs explored in this work, and the results obtained are summarised in Table 2.

The NPs prepared using acetylacetonates (FeCo_A) mainly led to the formation of CoO and CoFe$_2$O$_4$, although a weak peak of FeCo is present in the XRD diffractogram at 52.5° (Fig. 1a). Spherical NPs were produced with an average diameter of 5.1 ± 0.9 nm (Fig. 2A). Due to the simultaneous presence of the antiferromagnetic CoO, the saturation magnetization (M_s) is lower than that expected for pure cobalt ferrites, having a value of 28 A m^2 kg^{-1} (Fig. 1b). The XRD diffractogram reveals that mixed-phase NPs consisting of FeCo, CoFe$_2$O$_4$ and CoO were generated (Fig. 1C), when iron and cobalt oleate were used as precursors (FeCo_B). However, in that case, by comparing the relative intensities of CoFe$_2$O$_4$ and CoO peaks, one can notice that the CoFe$_2$O$_4$ phase is favoured over CoO. This is also corroborated by the higher M_s value (63 A m^2 kg^{-1} and 28 A m^2 kg^{-1} for FeCo_B and FeCo_A, respectively). Fig. 2B depicts the spherical morphology of these NPs, with a mean diameter of 5.9 ± 1.6 nm. The third set of precursors used was ferrocene and cobaltocene (FeCo_C). In that system, CoO is the NP main phase which has a direct impact on the M_s value (32 A m^2 kg^{-1}), as demonstrated in Fig. 1e and f. The TEM micrograph displays the spherical shape of the

Table 2 Synthesis of NPs using different precursor pairs

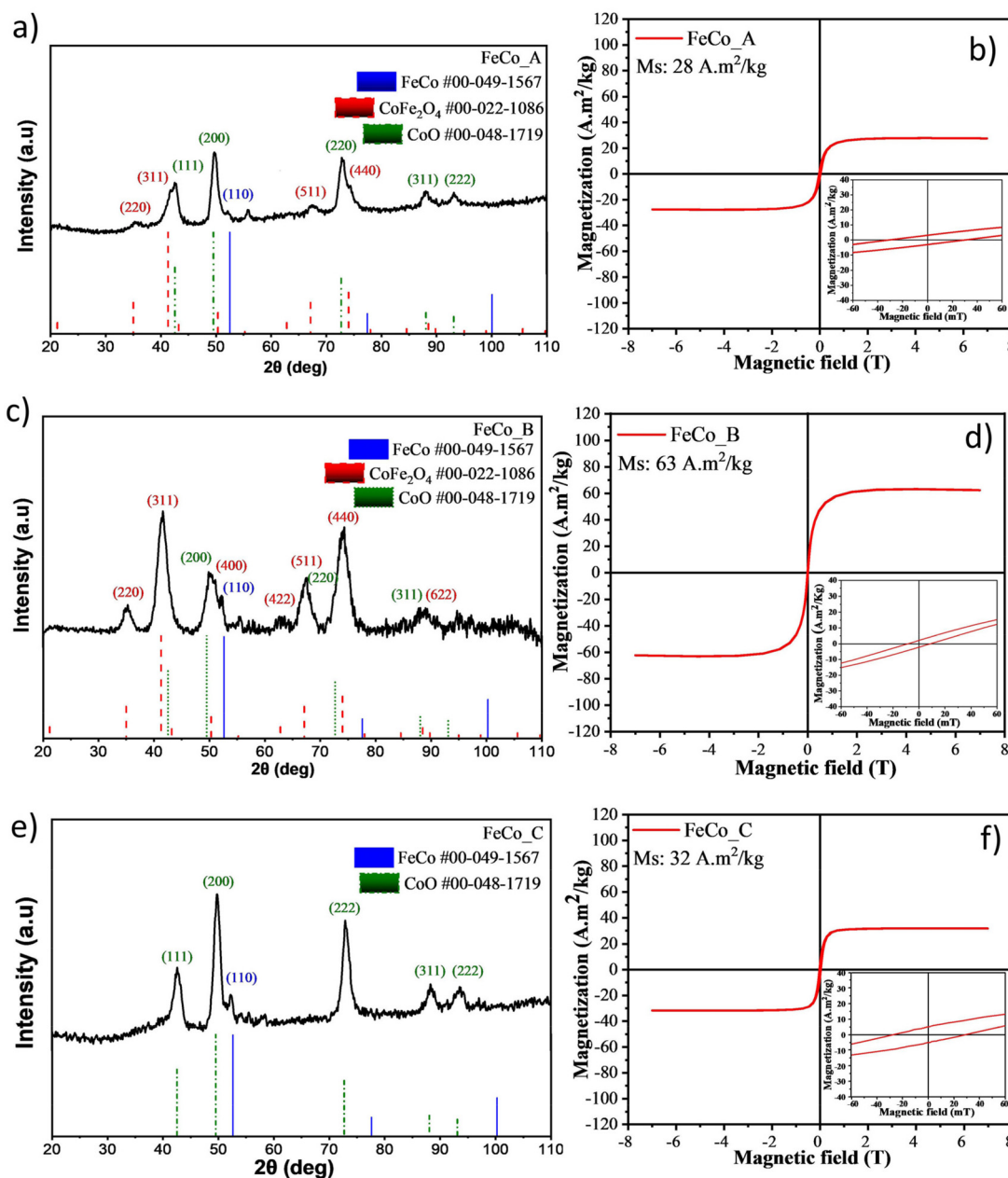| Synthesis	Precursors	Phases formed	Diameter (nm)	M_s (A m^2 kg^{-1})
FeCo_A	Fe(acac)$_3$, Co(acac)$_2$	CoFe$_2$O$_4$ and CoO	5.1 ± 0.9	28 ± 1
FeCo_B	Fe(ol)$_3$, Co(ol)$_2$	CoFe$_2$O$_4$ and CoO	5.9 ± 1.6	63 ± 3
FeCo_C	ferrocene, cobaltocene	CoO	9.4 ± 1.6	32 ± 2

Fig. 1 XRD and SQUID measurements of FeCo_A (a and b), FeCo_B (c and d) and FeCo_C (e and f). Insets: zoomed-in images of the hysteresis loop between −60 and +60 mT.

nanocrystals with an average diameter of 9.4 ± 1.6 nm (Fig. 2C). It is noted that in all syntheses reported above, and by observing the insets in Fig. 1, a soft ferromagnetic behaviour is indicated rather than a superparamagnetic one. Still, the resulting NPs are quite stable in their colloidal dispersions and no aggregation takes place.

In the literature, several precursor pairs have been studied also in a variety of different research endeavours involving the synthesis of cobalt ferrite NPs. Ramanavicius et al. produced hydrophilic 7.2 nm $CoFe_2O_4$ NPs stabilized by L-lysine using $FeCl_3$ and $CoCl_2$ salts as precursors. The thermal decompo-

sition of $Co(acac)_2$ and $Fe(acac)_3$ metal sources in the presence of oleic acid and trimethylamine-N-oxide resulted in the formation of 7.5 nm hydrophobic particles. The latter NPs had a higher saturation magnetization value (52 A m^2 kg^{-1}) compared to the particles similar in size which were coated by L-lysine (46 A m^2 kg^{-1}).[38] The combustion method employing $Co(NO_3)_2 \cdot 6H_2O$ and $Fe(NO_3)_3 \cdot 9H_2O$ led to the generation of 69.5 nm cobalt ferrite NPs with an M_s of 56.7 A m^2 kg^{-1}.[39] Malinowska et al. explored the influence of several precursor kinds (sulphates, chlorides and nitrates) employed to fabricate $CoFe_2O_4$ NPs. It was observed that larger particles (up to
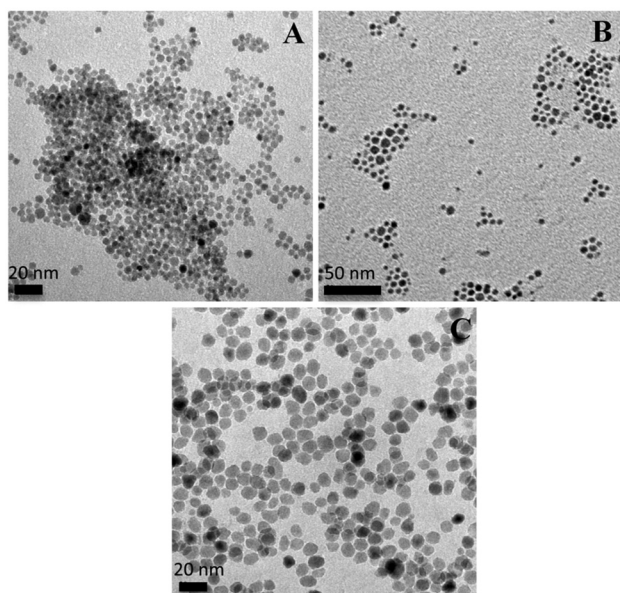
**Fig. 2** TEM images of samples FeCo_A (A), FeCo_B (B) and FeCo_C (C).

20 nm in crystalline grain size) were isolated when utilizing nitrates as metal sources in comparison with the case of chlorides and sulphates. The authors suggested that structural properties, lattice strain and particle clustering may be related to the observed variations of the mean particle size upon using distinct precursors. The produced particles were soft magnetic materials with typical ferrimagnetic features at room temperature. Metal sulphates provided $CoFe_2O_4$ NPs with the highest M_s (60 A m^2 kg^{-1}) among the three samples.[40] Guerioune and co-workers reported the synthesis of $CoFe_2O_4$ NPs by hydrothermal and co-precipitation methods employing nitrate, chloride and acetate precursors. Particles with a platelet morphology were generated with a mean size between 11 and 26 nm as a function of the synthetic parameters utilized. Hydrothermal synthesis in the presence of iron- and cobalt-nitrates provided NPs with a mean size of ~17 nm and a saturation magnetization of 63 A m^2 kg^{-1}. The authors discuss that the lower M_s than that of bulk $CoFe_2O_4$ (75.2 A m^2 kg^{-1}) is attributed to the small particle surface effect (spin canting) that becomes more significant as the particles become smaller in size.[41] In a work by Peterlik and co-workers, the smallest cobalt NPs were obtained by a simple and rapid sol–gel approach starting from nitrate salts (40–41 nm) and by co-precipitation with carbonate in the presence of a small quantity of polydimethylsiloxane.[42] On the other hand, it has to be noted that Christensen and co-workers used three different cobalt sources, *i.e.* $CoCl_2$, $Co(NO_3)_2$ and $Co(CH_3COOH)_2$ in combination with $Fe(NO_3)_3 \cdot 9H_2O$ as a common iron precursor: the produced cobalt ferrite NP samples displayed practically identical crystal and magnetic structures; only unit-cell parameters, thermal vibrations and magnetic moments exhibited slight variations.[43] Thanh and co-workers reported the synthesis of $CoFe_2O_4$ NPs by thermal decomposition of iron(III) and cobalt(II)

acetylacetonates in organic solvents using OAc and OAm as surfactants while HDD or octadecanol played the role of an accelerating agent. Nanostructures with varying morphologies and monodisperse sizes in the range 7–30 nm were isolated by that approach. Saturation magnetization values were in the range 51–64 A m^2 kg^{-1} for the different samples.[1] Baaziz *et al.* demonstrated that using metal oleates and stearates in the presence of OAc favored the creation of core–shell $Co_xFe_{1-x}O@Co_yFe_{3-y}O_4$ NPs, which was attributed to the reducing action offered by oleate groups from the OAc and precursors. These researchers observed the formation of 15 nm $CoFe_2O_4$ nanocubes upon using mixed oleate generated *in situ* from metal iron chloride and cobalt chloride in the presence of Na-oleate. The M_s of the nanocube sample at 5 K was 68 A m^2 kg^{-1}.[44]

As can be seen from our current results shown above, regardless of the choice of the precursor, the synthesis of single phase NPs did not flourish under the tested conditions. FeCo NPs are chemically unstable and prone to oxidation. Therefore, a reductive annealing procedure was adopted to ensure phase transformation and produce single phase FeCo nanocrystals.[45] The salt-matrix annealing procedure was first applied to the as-synthesised FeCo_C NPs and then we tried to improve it in subsequent syntheses. The NPs were mixed with NaCl with a NP to salt weight ratio of 1 : 1000 and then annealed at 500 °C for 1 h (FeCo@C_C) under a reducing gas flow. XRD measurements confirm that the annealed NPs are composed of single phase FeCo, whereas the M_s is dramatically increased from 32 to 182 A m^2 kg^{-1}. They further rule out the presence of residual NaCl, as no sodium chloride peaks are spotted on the XRD diagram (Fig. 3b), and evidence the effectiveness of the washing procedure. However, there is a significant enhancement of the particle size as well. The NPs are now polydisperse and the sintering effect has taken place (Fig. 3c and d). The hysteresis loop is also modified, indicating a ferromagnetic behaviour (coercivity: 61 mT, remanent magnetization: 45 A m^2 kg^{-1}). It seems reasonable to assume that the presence of amorphous Fe or Fe-rich FeCo entities in the CoO-rich sample before annealing remained undetected by XRD, while during annealing this amount of iron could blend well with cobalt to yield the crystalline and strongly magnetic FeCo alloy. In any case, STEM-EDX analysis confirms that the atomic % of Fe is comparable to that of Co in the as-prepared FeCo_C sample, as presented in Fig. S1 of the ESI.† ICP-AES measurements are in agreement with STEM-EDX results within uncertainty, revealing a nearly stoichiometric 50.7% Fe/49.3% Co atomic ratio.

The increase of the M_s value can be mainly attributed to the formation of large FeCo nanocrystals (bulk FeCo M_s: 240–245 A m^2 kg^{-1}) and to the fact that the annealing process may lead to a homogeneous atomic distribution of iron and cobalt within individual NPs, endowing an increased crystallinity. This procedure results in the formation of a carbon shell around the surface of the particles, which could potentially prevent them from sintering, at least to some extent.[30,46] As shown in Fig. 3d, indeed there is a shell around the NPs but
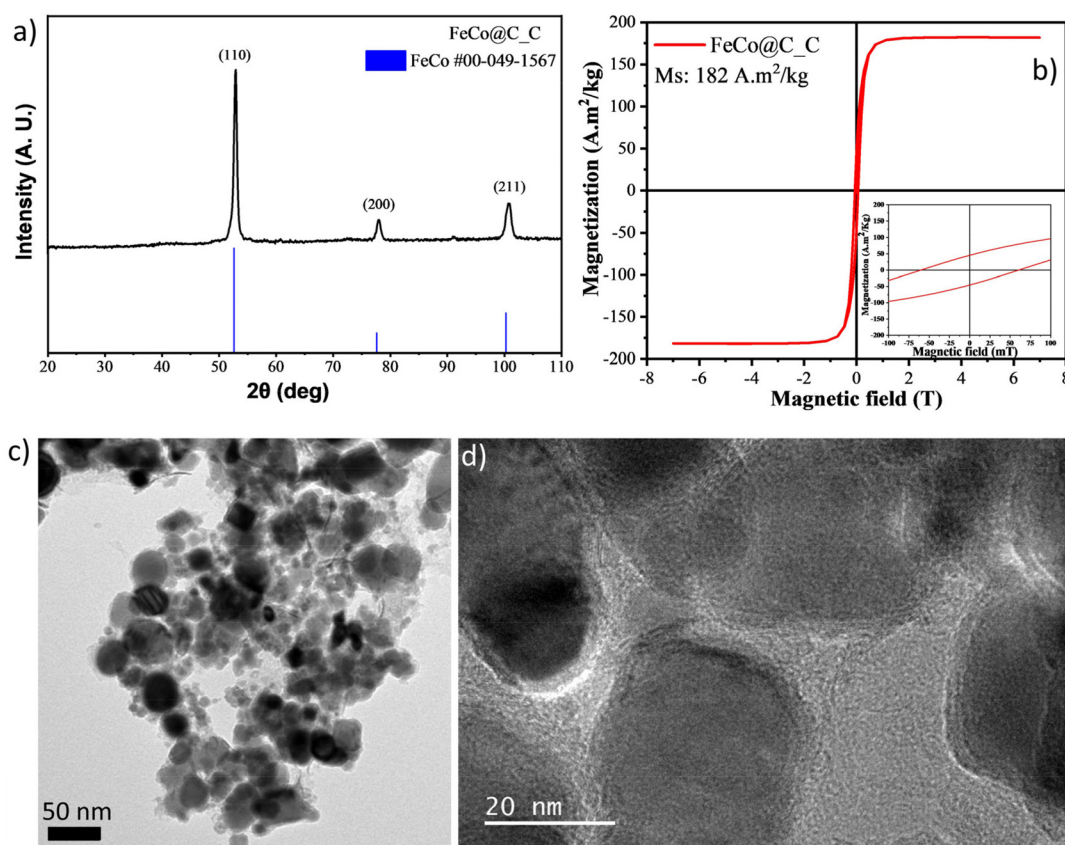
Fig. 3 XRD (a) and SQUID (b) measurements and TEM images (c and d) after annealing (FeCo@C_C). Inset: close look of the M–H plot between −100 and 100 mT.

the sintering has not been avoided. It is worth noting that apart from reductive annealing, oxidative annealing in the presence of air instead of a N_2/H_2 mixture has also been reported elsewhere as an approach to adjust the oxidation state of magnetic nanoparticles.[47]

3.2. Synthesis of $CoFe_2O_4$ NPs from acetylacetonate precursors – the role of ligands and additives

In order to investigate how the existence of ligands/reagents (OAm, HDD) affects the morphology and composition of the particles, we performed two syntheses changing one parameter per experiment, while keeping the rest of the conditions constant. In this set of experiments, we used the acetylacetonate precursors, considering FeCo_A (section 3.1) as the control sample. The results are summarised in Table 3.

As XRD patterns reveal (Fig. 4a), the synthesis without oleylamine (FeCo_E) led mainly to the formation of $CoFe_2O_4$ and CoO. ICP measurements revealed a Co-rich composition (23.3 vs. 76.7 atomic % for Fe vs. Co, respectively), which is in accordance with the presence of an additional CoO phase. Still, comparing the relative intensities of the main peaks of $CoFe_2O_4$ (at 41°) and CoO (at 49°) of FeCo_A (where both OAc and OAm were used, Fig. 1a) and FeCo_E, one can observe that by omitting OAm, the acquisition of the $CoFe_2O_4$ phase was promoted while CoO amount was somewhat decreased. Moreover, the size of NPs was also increased from 5.1 ± 0.9 to 7.2 ± 1 nm (Fig. 5A). Due to the presence of CoO, the M_s value is low but higher than that in the control synthesis (43 A m² kg⁻¹ and 28 A m² kg⁻¹, respectively), since in the former case the particles are larger with enhanced $CoFe_2O_4$ phase content (Fig. 4b).

Table 3 Parametric study of the synthesis of $CoFe_2O_4$ NPs from a metal acetylacetonate precursor pair

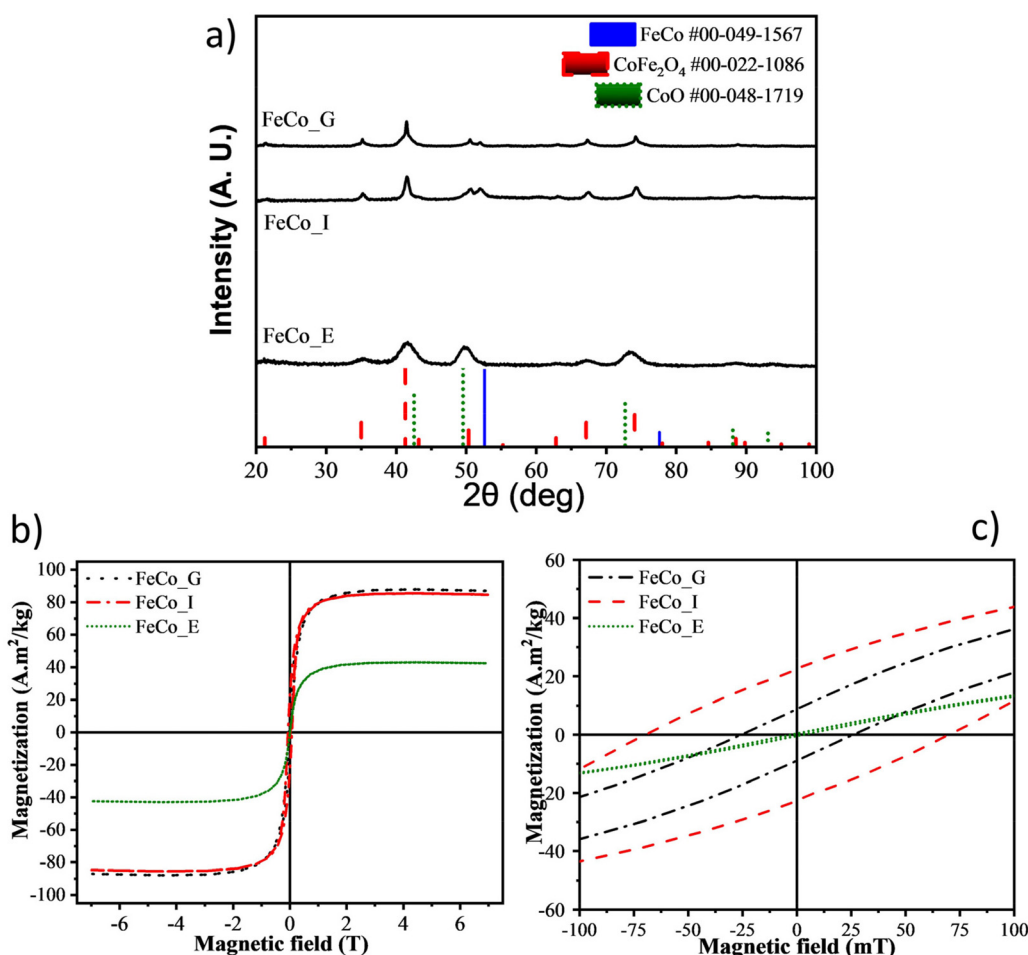| Synthesis	Parameter changed	Phase content	Diameter (nm)	M_s (A m² kg⁻¹)
FeCo_A	None (control samples)	$CoFe_2O_4$ and CoO	5.1 ± 0.9	28 ± 1
FeCo_E	No oleylamine	$CoFe_2O_4$ and CoO	7.2 ± 1	43 ± 2
FeCo_G	No oleic acid	$CoFe_2O_4$	5.9 ± 0.8	88 ± 4
FeCo_I	No HDD	$CoFe_2O_4$	46.5 ± 5.2 (clusters)	85 ± 4

Fig. 4 XRD diffractograms (a) and SQUID measurements (b) for the three samples prepared with M-acac precursors. Graph c is a zoom in of hysteresis loops between −100 and 100 mT.

The next step was to explore how the reaction time could affect the formation of NPs. Extending the reaction time from 1 to 3 h (sample FeCo_G) implies that the NPs are exposed for longer time to a high temperature and reducing atmosphere (N_2/H_2 gas). As shown in Fig. 4a, XRD analysis denotes the formation of $CoFe_2O_4$ nanocrystals. In terms of morphology, monodisperse spherical particles were produced (Fig. 5B), with an average diameter of 5.9 ± 0.8 nm. By prolonging the reaction time to 3 h, the NPs produced were slightly larger with lower size distribution (12.6% and 17.6% for FeCo_G and FeCo_A, respectively). The sample FeCo_G demonstrated an M_s value of 88 A m² kg⁻¹, which is similar within uncertainty to the reported M_s value of bulk $CoFe_2O_4$ (80–85 A m² kg⁻¹).[1,18]

Hexadecanediol acts as an accelerating agent for the thermal decomposition of acetylacetonate precursors. Lu *et al.* suggests that the presence of HDD improves the monodispersity and yield of the reaction.[1] The synthesis in the absence of HDD (FeCo_I) led to the production of multicore (cluster) NPs (Fig. 5c and d). Multicore nanocrystals are particularly attractive structures for biomedical applications. Due to their internal collective organisation, they increase the heating

efficiency in magnetic fluid hyperthermia and provide better contrast enhancement in MRI, compared to single-core particles.[48–50] The as-synthesised particles are mainly composed of $CoFe_2O_4$, while a weak peak of FeCo is also present (Fig. 4a). The latter finding seems to be in reasonable agreement with ICP results, which yielded a 53.3% Fe/46.7% Co atomic ratio. These nanostructures have a size of 46.5 ± 5.2 nm (10–15 nm single particle size) and an M_s value of 85 A m² kg⁻¹ (Fig. 4b). Fig. 4b and c show the hysteresis loop for the syntheses reported above. The hysteresis loop is almost absent for the sample FeCo_E, indicating superparamagnetic behavior, while it is more prominent for the sample FeCo_I.

3.3. Study of the annealing procedure

As described previously, a salt-matrix annealing procedure was adopted to achieve phase transformation from cobalt ferrite-cobalt oxide to FeCo. FeCo_C NPs were reduced to FeCo when annealed at 500 °C. Their magnetic properties have been significantly increased but agglomeration was observed (section 3.1). In the next set of the experiments, we examined the annealing procedure at different temperatures and reaction
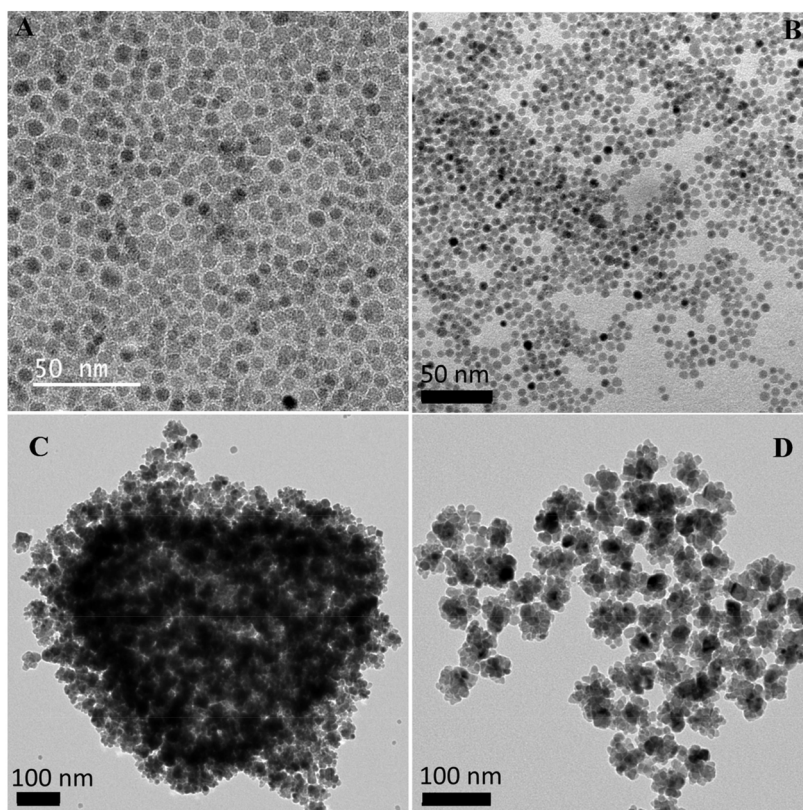
Fig. 5 TEM images of samples FeCo_E (A), FeCo_G (B) and FeCo_I (C and D).

times, as described in Table 4. For this study we used the FeCo_G particles (section 3.2).

When annealing the particles at 450 °C for 1 h (FeCo_G@450_1 h), the phase transformation is incomplete as witnessed by the XRD pattern (Fig. 6). The weak peaks at 41° and 74° indicate a residual $CoFe_2O_4$ phase. The NPs were almost completely reduced to FeCo when the reaction time was increased to 2 h (FeCo_G@450_2 h). However, the M_s value (121 A m^2 kg^{-1}) is lower than that of bulk FeCo (240–245 A m^2 kg^{-1}). In both cases the samples are polydisperse and agglomeration occurs (Fig. 7A and B). The annealing treatment was then applied at 350 °C to examine whether by using lower temperature the aggregation or severe coalescence can be prevented. As the XRD diffractogram shows (FeCo_G@350_2 h), the formation of the FeCo phase was significantly boosted after annealing but still the $CoFe_2O_4$ phase is the dominant one, which is in agreement with the measured M_s value (94 A
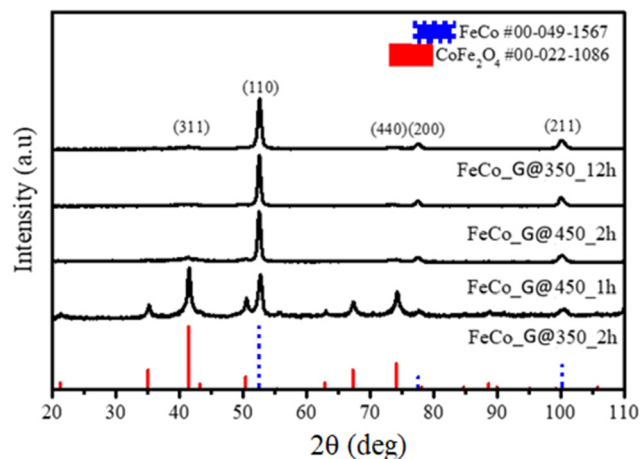

Fig. 6 XRD measurements of the annealed FeCo_G NPs at different temperatures and reaction times.

m^2 kg^{-1}). To ensure phase transformation, we extended the reaction time to 12 h (FeCo_G@350_12 h). Nevertheless, Fig. 7C and D illustrate that even at lower temperature the NPs tend to agglomerate and the samples are polydisperse. Cannas *et al.* have also reported that the heating treatment at very high temperatures can lead to the progressive increase of the particle size and the structural ordering of the samples. If the samples are diluted, then the matrix (*e.g.* a silica matrix) can

Table 4 Annealing of sample FeCo_G at different temperatures and reaction times

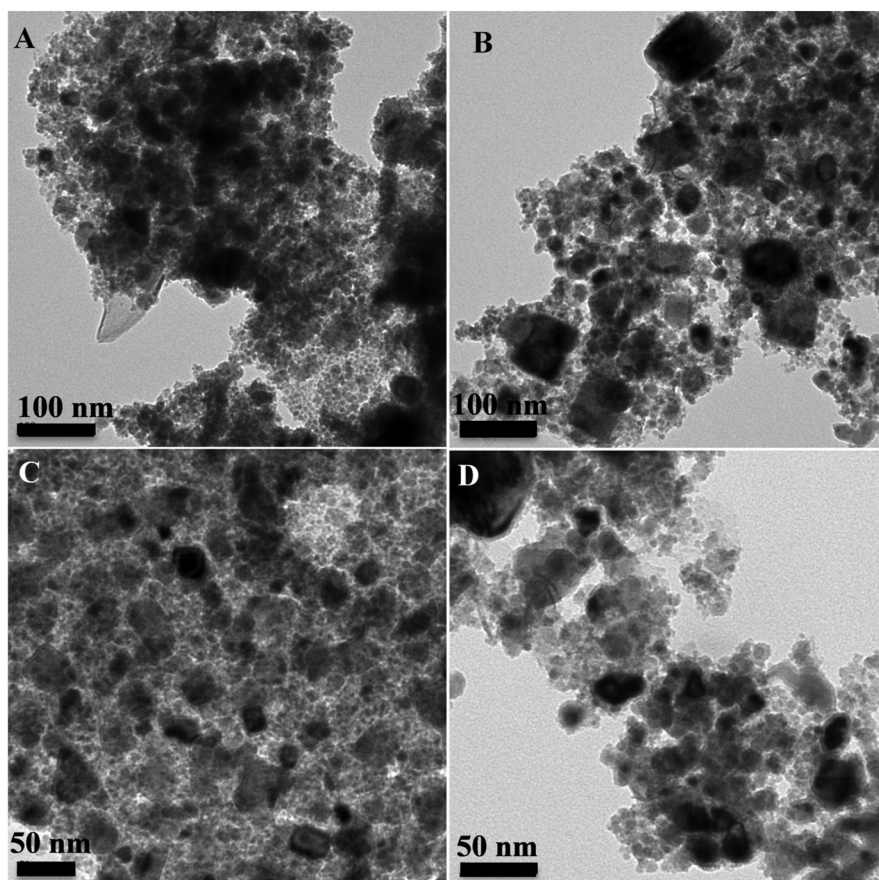| Synthesis	Temperature	Reaction time	M_s (A m^2 kg^{-1})
FeCo_G@450_1h	450 °C	1 h	100 ± 5
FeCo_G@450_2h	450 °C	2 h	121 ± 6
FeCo_G@350_2h	350 °C	2 h	94 ± 5
FeCo_G@350_12h	350 °C	12 h	108 ± 5

Fig. 7 TEM images of the samples FeCo_G@450_1 h (A), FeCo_G@450_2 h (B), FeCo_G@350_2 h (C) and FeCo_G@350_12 h (D).

even prevent particle aggregation. However, the particles can be still composed of $CoFe_2O_4$ after calcination, and not of FeCo.[51] Probably in our case the use of a slightly reducing atmosphere (presence of a small portion of H_2) was responsible for the partial reduction to FeCo. Still, even if cobalt ferrite remains the prevalent phase in the nanoparticles after annealing, an increase of the magnetization of the samples as a function of the annealing temperature is commonly observed, as reported by Garcia Cerda and Montemayor.[52]

3.4. Synthesis of FeCo NPs using the polyol method

The polyol method is a commonly employed synthetic approach which can be utilized to produce hydrophilic NPs. This strategy involves the use of a polyhydric alcohol (polyol) as a solvent, which also serves as a surfactant.[53,54] Sodium hydroxide (NaOH), when added in sufficient concentration, generates glycolate anions by deprotonation of the glycol, which acts as a reducing agent of the metallic precursors.[20] Zamanpour *et al.* reported size-controlled synthesis of FeCo nanocrystals (20–30 nm) with high magnetization (*ca.* 220 A m^2 kg^{-1}) by adjusting the molar ratio of NaOH to precursors, and the reaction time.[55] Based on that protocol, we performed four syntheses aiming to produce small FeCo NPs in the presence of iron chloride, cobalt acetate and ethylene glycol at 200 °C (Table 5).

Table 5 Synthesis of FeCo NPs with the polyol method

Synthesis	NaOH : precursor ratio	Reaction time	M_s (A m^2 kg^{-1})
FeCo_p1	27	25 min	182 ± 9
FeCo_p2	10	10 min	190 ± 10
FeCo_p3	10	1 h	156 ± 8
FeCo_p4	40	25 min	196 ± 10

Although our experimental findings do not corroborate the previously reported results in terms of size of the particles formed (only particles larger than 100 nm were obtained, Fig. 8b and S2b†), the polyol synthesis indeed led to the formation of FeCo nanocrystals with high magnetization (up to 200 A m^2 kg^{-1}). Indicative results are shown in Fig. 8 and Fig. S2.† The XRD patterns reveal the formation of cobalt-rich FeCo particles (Co_7Fe_3, ICDD: 050-0795) for the sample FeCo_p2 (Fig. 8a). ICP measurements demonstrated a 25% Fe/75% Co atomic ratio, corroborating the presence of a Co-rich alloy phase. During the FeCo_p4 synthesis, a Co phase is also present to a much lower degree, together with a Fe-rich alloy phase (Fe_7Co_3, ICDD: 048-4816, Fig. S2a†). This composition is supported by ICP results, which provided a 63.2% Fe/36.8% Co atomic ratio. In our experiments, large >100 nm NPs were produced with the polyol method for both of the above
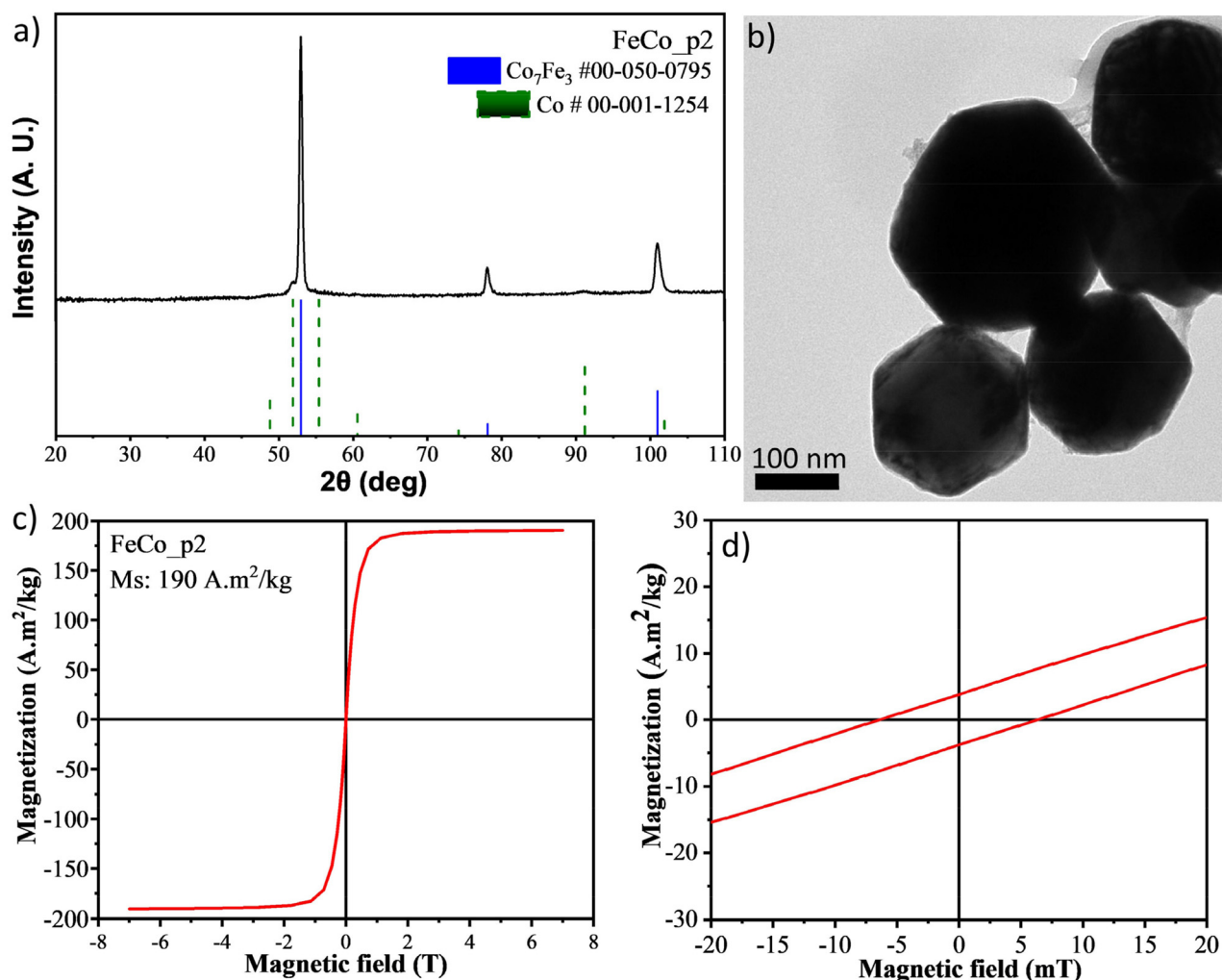
Fig. 8 (a) XRD measurement, (b) TEM image and (c) SQUID measurement for the sample FeCo_p2, (d) a close look of the M-H plot between −20 and 20 mT.

samples, demonstrating a hexagonal morphology (Fig. 8b and S2b†). Even though the remanent magnetization and coercivity are not high, the particles cannot be deemed as superparamagnetic but their magnetic behavior can be better classified as soft ferromagnetic, with coercivity values below 8 mT (Fig. 8d and Fig. S2d†). It is well established that producing large FeCo particles is more feasible than the formation of smaller particles (less than 20 nm). In the former case, an oxide shell is formed on the surface of the bigger nanocrystals, which protects them from further oxidation, acting in a passivating way. In the latter case, due to the larger surface area, oxidation occurs quickly, spreading through the entire volume of the particle and affording cobalt ferrite.

For example, Tomar and Jeevanandam prepared Co–Fe glycolates by refluxing cobalt acetate tetrahydrate and Fe(acac)$_3$ in EG, in the absence of NaOH. CoFe$_2$O$_4$ particles formed under these conditions, with size below 21 nm, while some samples consisted of larger octahedral and hexagonal particles which however were made up of smaller cobalt ferrite NPs.[59] The

same researchers have studied also the roles of different cobalt precursors (cobalt acetate, cobalt acetylacetonate, cobalt chloride and cobalt nitrate) in the synthesis of Co–Fe glycolates and produced <20 nm CoFe$_2$O$_4$ NPs. Cobalt ferrite NPs were also generated when both metallic precursors were chloride ones, i.e. FeCl$_3$·6H$_2$O and CoCl$_2$·4H$_2$O, after refluxing the reaction mixture in EG, diethylene glycol (DEG) or triethylene glycol (TEG).[60] Synthesis in TEG for 3 h led to the acquisition of impurity-free 6–11 nm large NPs.[61] Interestingly, Ardisson and co-workers reported the synthesis of very small (<5 nm) citrate-capped cobalt ferrite NPs with superior colloidal stability via a one-step route in the presence of iron(III) chloride nonahydrate, cobalt(II) chloride hexahydrate, trisodium citrate, NaOH and DEG at 245 °C.[62] In all cases, the magnetization values reported were in the 37–52 A m^2 kg^{-1} range, as expected for cobalt ferrite. It seems that in our case, the hydroxyl ions supplied by NaOH provided nucleation sites for FeCo NPs during the polyol process.[55,63] The big size (>100 nm) of our particles appears to be crucial for their lack of severe oxidation, and

thus for their much higher magnetization, in comparison with those in the above-mentioned literature works; for example, Ardisson and colleagues[62] also used NaOH, but the small size of their particles was probably responsible for the cobalt ferrite composition that they observed, rather than a bimetallic FeCo alloy. It seems that the reducing ability of polyols cannot fully prevent nanoparticle oxidation if the particle size is relatively small.

The FeCo NPs produced as described herein are not ideal for *in vivo* applications owing to their large size, but high magnetization particles can be extremely useful for other applications such as magnetic separation[56] and high-density recording media.[57,58]

3.5. Synthesis of FeCo NPs under a H₂ atmosphere and application in hyperthermia

Aiming to synthesize bimetallic FeCo NPs with a minimum degree of surface oxidation, while keeping the particle size at a controlled level, a hydrogen atmosphere was applied during synthesis. Gases like H_2 can have easy diffusion in solids and solutions, despite their low solubility in many solvents. Hydrogen gas serves as a reducing agent to produce NPs with the advantage of leaving behind little or no residues on the particle surface. H_2, being a mild reductant, permits a fine tailoring of the reduction rate, and by adjusting the reaction temperature at 'moderate' levels, the particle growth can be tuned to a satisfactory extent,[64] often avoiding the occurrence

of uncontrolled growth to huge or very polydisperse particle sizes. Under the employed synthetic conditions, in the presence of OAc and HDA surfactants, the resulting mean particle size was measured at 30.3 ± 4 nm (Fig. 9). Monodisperse NPs with a hexagonal-like shape can be observed, with STEM-EDX elemental mapping demonstrating a homogeneous distribution of Fe and Co elements throughout the particle volume. HRTEM and STEM imaging reveals the presence of a surface layer with a brighter contrast surrounding the particles, presumably consisting of (amorphous) cobalt ferrite or iron oxide. From the M–H loops presented at Fig. 10a, a normalized saturation magnetization M_s of ~145 A m² kg⁻¹ at room temperature is derived, with a coercivity of *ca.* 2.5 mT. Such magnetic characteristics indicate a soft ferromagnetic behaviour, with nearly superparamagnetic features. The XRD diffractogram shown in Fig. 10b illustrates that the particles are mostly composed of an Fe_xCo_y alloy (not excluding the presence of oxides), considering the main peak at approximately 50.8°. The aforementioned value for the saturation magnetization is lower than those reported for the polyol-prepared samples presented in Table 5. This can be attributed to the smaller particle size in the sample under discussion (produced with H_2 reductant) as well as its largely amorphous composition, implied by the XRD and selected area electron diffraction (SAED) (Fig. 9B inset) measurements; in particular, a crystalline grain size of less than 2 nm is derived by applying Scherrer's equation at the dominant XRD peak, whereas the TEM particle size
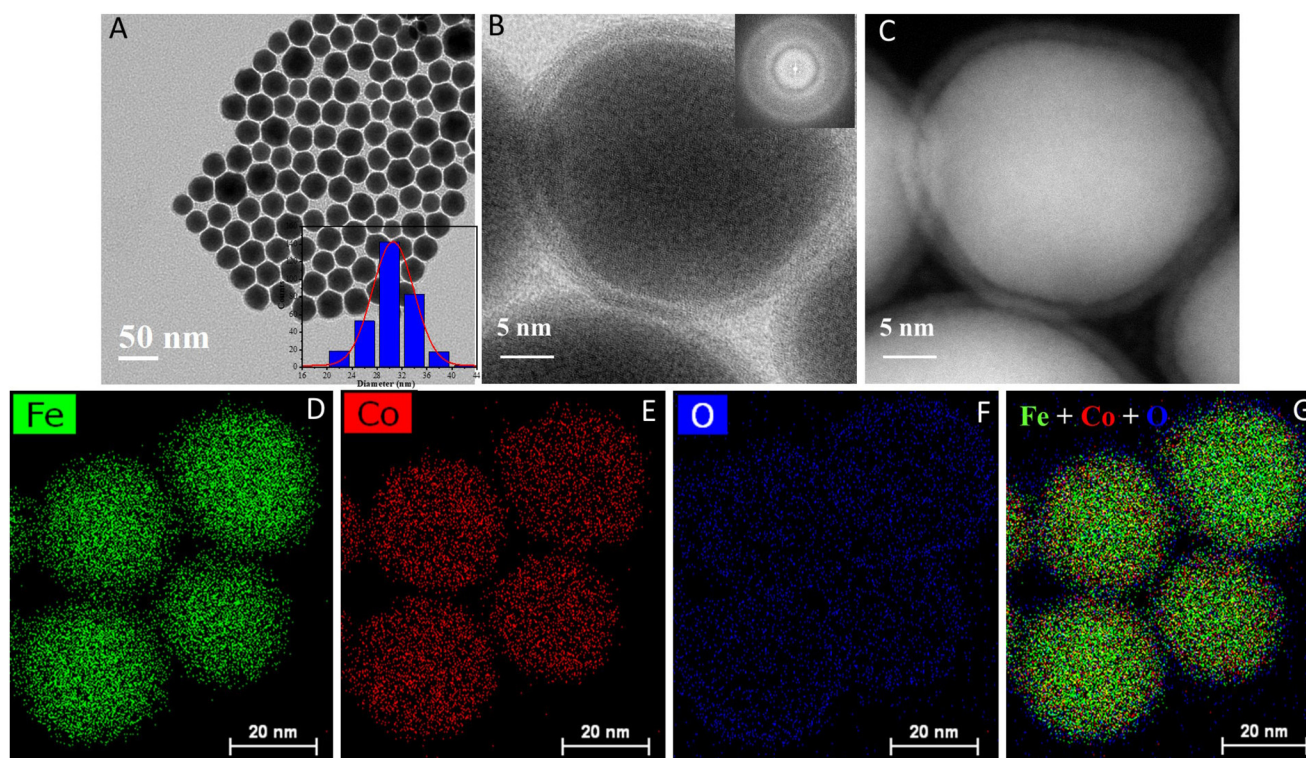
Fig. 9 Electron microscopy characterization of the H₂-produced FeCo NPs: TEM image and size histogram as inset (A); HRTEM image with the SAED pattern as inset (B); HAADF-STEM image (C); HAADF-STEM-EDX elemental mapping for the different elements (D–F); and overlapping maps (G).
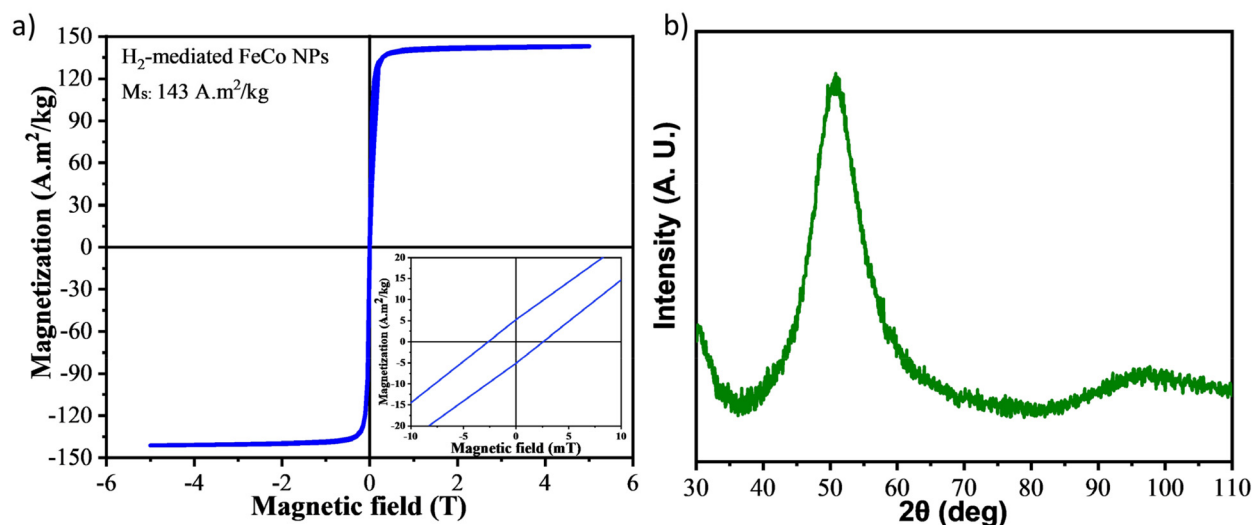
Fig. 10 (a) SQUID measurement recorded at room temperature and (b) XRD diffractogram for the H$_2$-mediated FeCo NPs. The inset in (a) shows a zoom in of low values of magnetic field.

reaches 30 nm, as mentioned above. At the same time, diffuse rings in the SAED pattern are assigned to the significant poly-crystalline/amorphous portions of the sample.

The heating ability of the H$_2$-produced FeCo NPs, which present the highest magnetization and a size compatible with biomedical applications, was evaluated by testing particle dispersions. Magnetic field hyperthermia was employed to assess the efficiency of the particles to generate heat. Evaluating the heating ability in particle dispersions, rather than in the solid state, is the most common way of hyperthermia measurement, followed by the majority of research groups studying the heating properties of magnetic nanoparticles. To achieve water dispersibility, the particles were functionalized with DSPE-PEG.

DSPE-PEG. The functionalized NPs showed high colloidal stability with a hydrodynamic diameter (D_h) of 118.2 ± 23.1 nm and a ζ-potential of −25.9 ± 5.5 mV at pH 6.5 (Fig. 11A). In fact, the ability of DSPE-PEG to provide hydrophilicity to iron oxide magnetic nanoparticles had already been reported by Bao and co-workers in 2004.[65] The DSPE-PEG micelle coating method entails the interaction between the residual hydrophobic capping ligands on the surface of the NPs and the amphiphilic PEG-phospholipids. The surface-exposed hydrophilic PEG chains offer good solubility of the coated iron oxide NPs.[65] The end groups of DSPE-PEG can be easily grafted to different targeting moieties such as peptides, antibodies and non-antibody ligand-targeting moieties.[65,66] Such further modi-
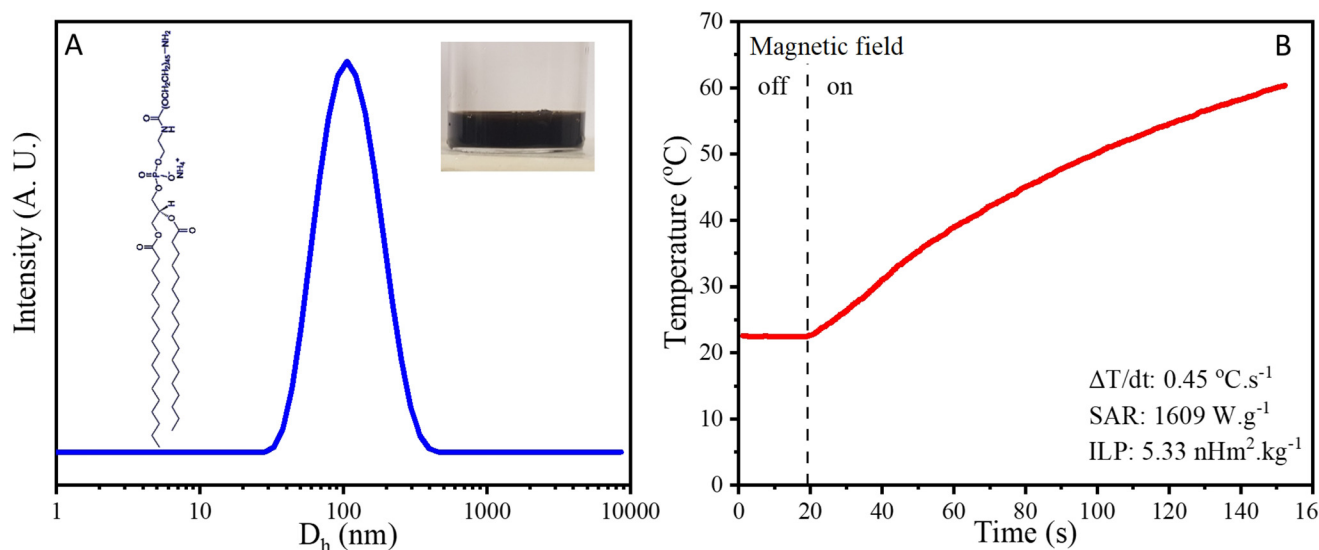
Fig. 11 DLS measurement of surface-functionalized water-dispersible FeCo NPs (A); heating efficiency of the NPs upon applying an AC magnetic field (B).

fications with relevant biomolecules can be interesting for applications such as hyperthermia, drug delivery and specific recognition of tumoral cells. For schematic representations of the development of DSPE-PEG surface-treated magnetic NPs and their posterior functionalizations see also ref. 65.

The results regarding the SAR of our FeCo NPs are illustrated in Fig. 11B, revealing that the NPs possess an outstanding heating efficiency. More specifically, the SAR exceeds 1600 W g^{-1}, which is a comparable or even higher value compared to SAR values reported in the literature for other H_2-mediated FeCo nanoparticles.[67] To better understand the origin of this remarkable heating performance, the previously discussed magnetic and structural characteristics of the FeCo nanoparticles can be examined in light of known magnetic regimes. The particle size places them within the single-domain range expected for FeCo alloys–between the critical diameters for the superparamagnetic-to-ferromagnetic transition (~16 nm) and multi-domain formation (~51 nm).[68] This, combined with their soft ferromagnetic character and near-equiatomic FeCo composition (50.2 wt% Fe, 49.8 wt% Co, as confirmed by ICP-AES), strongly supports a single-domain ferromagnetic state. Such a regime is known to favor efficient heat generation *via* hysteresis losses under alternating magnetic fields. Similar conclusions were drawn in a study by Lacroix *et al.*,[69] where smaller FeCo nanoparticles (~14 nm) exhibited ferromagnetic behavior and significant energy losses, even with similarly reduced (below the bulk) magnetization values (~144 A m^2 kg^{-1}). In systems like these, the assumptions of linear response theory no longer apply, and the Stoner–Wohlfarth (SW) model becomes a more suitable framework, as it accounts for coherent magnetization reversal in single-domain particles. Thus, although dynamic magnetic measurements were not performed, the combination of structural, compositional and static magnetic data clearly supports the conclusion that the observed high SAR arises from hysteresis-driven heating in blocked, single-domain FeCo NPs consistent with SW-type behavior.

It should be emphasized that this work does not involve *in vitro* or *in vivo* experimentation. The primary objective in this section was to investigate the magnetic heating performance of the synthesized FeCo nanoparticles and evaluate their potential suitability for future hyperthermia applications. In this context, the applied magnetic field and frequency were selected to effectively characterize the heat generation capabilities of the particles. To enable comparison with other nanoparticle systems tested under different experimental conditions, we report the intrinsic loss power (ILP), calculated as 5.33 nH m^2 kg^{-1}. The ILP is a parameter that provides a standardized measure of the nanoparticle heating efficiency, independent of the applied alternating magnetic field amplitude and frequency. This allows a more objective assessment of the heating potential of the FeCo MNPs and supports their consideration for further development in magnetic hyperthermia contexts.

The calculated ILP for the FeCo NPs (5.33 nH m^2 kg^{-1}) is notably higher than the values typically reported for iron oxide or ferrite-based systems, which often range between 0.5 and 3 nH m^2 kg^{-1}.[70] This confirms their superior intrinsic heating efficiency and highlights the advantages of FeCo alloys in magnetic hyperthermia. The elevated ILP reflects the combination of high magnetic moment, optimal particle size within the single-domain regime, and favorable soft ferromagnetic properties. These characteristics position the synthesized FeCo nanoparticles as strong candidates for high-performance magnetic hyperthermia applications.

4. Conclusions

Various reaction parameters have been studied in detail concerning the synthesis of $CoFe_2O_4$-based and FeCo NPs. Monodisperse spherical nanocrystals with a size of 5–8 nm were produced ($\sigma < 15\%$), demonstrating higher M_s values than those commonly reported in the literature. Multicore NPs were also prepared, which are promising for biomedical applications, such as MH and MRI. The study of the post-synthetic thermal treatment reveals complete phase transformation (from $CoFe_2O_4$ to FeCo) at 500 °C. However, the size of the annealed particles increases dramatically and aggregation takes place. The polyol method led to the formation of large FeCo NPs (>100 nm) with a hexagonal shape. By comparison with the literature, it was suggested that small (<10 nm) FeCo NPs are often unstable compared to large ones, being susceptible to air oxidation and conversion to $CoFe_2O_4$. H_2-mediated FeCo NPs with a mean size of ~30 nm which were further functionalized to achieve water dispersibility demonstrated excellent heating ability, denoting their high potential for magnetic field hyperthermia for cancer treatment.

Data availability

The data within this study are included in either the main article or ESI figures.†

Conflicts of interest

There are no conflicts to declare.

Acknowledgements

References

1 L. T. Lu, N. T. Dung, L. D. Tung, C. T. Thanh, O. K. Quy, N. V. Chuc, S. Maenosono and N. T. K. Thanh, Synthesis of

magnetic cobalt ferrite nanoparticles with controlled morphology, monodispersity and composition: the influence of solvent, surfactant, reductant and synthetic conditions, *Nanoscale*, 2015, **7**, 19596–19610.

2 R. Jasrotia, J. Prakash, Y. B. Saddeek, A. H. Alluhayb, A. A. Younis, N. Lakshmaiya, C. Prakash, K. A. Aly, M. Sillanpaa, Y. A. M. Ismail, A. Kandwal and P. Sharma, Cobalt ferrites: structural insights with potential applications in magnetic, dielectrics and catalysis, *Coord. Chem. Rev.*, 2025, **522**, 216198.

3 S.-h. Noh, W. Na, J.-t. Jang, J.-H. Lee, E. J. Lee, S. H. Moon, Y. Lim, J.-S. Shin and J. Cheon, Nanoscale Magnetism Control via Surface and Exchange Anisotropy for Optimized Ferrimagnetic Hysteresis, *Nano Lett.*, 2012, **12**, 3716–3721.

4 P. Sahoo, P. Choudhary, S. S. Laha, A. Dixit and O. Thompson, Mefford. Recent advances in zinc ferrite ($ZnFe_2O_4$) based nanostructures for magnetic hyperthermia applications, *Chem. Commun.*, 2023, **59**, 12065.

5 M. G. Naseri, E. B. Saion, H. A. Ahangar, M. Hashim and A. H. Shaari, Synthesis and characterization of manganese ferrite nanoparticles by thermal treatment method, *J. Magn. Magn. Mater.*, 2011, **323**, 1745–1749.

6 D. S. Raie, I. Tsonas, M. Canales, S. Mourdikoudis, K. Simeonidis, A. Makridis, D. Karfaridis, S. Ali, G. Vourlias, P. Wilson, L. Bozec, L. Ciric and N. T. K. Thanh, Enhanced detoxidication of Cr^{6+} by *Shewanella oneidensis* via adsorption on spherical and flower-like manganese ferrite nanostructures, *Nanoscale Adv.*, 2023, **5**, 2897–2910.

7 C. Liu, B. Zou, A. J. Rondinone and Z. J. Zhang, Chemical control of superparamagnetic properties of magnesium and cobalt spinel ferrite nanoparticles through atomic level magnetic couplings, *J. Am. Chem. Soc.*, 2000, **122**, 6263–6267.

8 A. M. El-Khawaga, M. Ayman, O. Hafez and R. E. Shalaby, Photocatalytic, antimicrobial and antibiofilm activities of $MgFe_2O_4$ magnetic nanoparticles, *Sci. Rep.*, 2024, **14**, 12877.

9 L. M. Lacroix, N. F. Huls, D. Ho, X. Sun, K. Cheng and S. Sun, Stable single-crystalline body centered cubic Fe nanoparticles, *Nano Lett.*, 2011, **11**, 1641–1645.

10 A. J. McGrath, S. Cheong, A. M. Henning, J. J. Gooding and R. D. Tilley, Size and shape evolution of highly magnetic iron nanoparticles from successive growth reactions, *Chem. Commun.*, 2017, **53**, 11548–11551.

11 K. D. Gilroy, A. Ruditskiy, H. C. Peng, D. Qin and Y. Xia, Bimetallic Nanocrystals: Syntheses, Properties, and Applications, *Chem. Rev.*, 2016, **116**, 10414–10472.

12 J. K. Mathiesen, H. M. Ashberry, R. Pokratath, J. T. L. Gamler, B. Wang, A. Kirsch, E. T. S. Kjaer, S. Banerjee, K. M. O. Jensen and S. E. Skrabalak, Why colloidal syntheses of bimetallic nanoparticles cannot be generalized, *ACS Nano*, 2024, **18**, 26937–26947.

13 C. Desvaux, F. Dumestre, C. Amiens, M. Respaud, P. Lecante, E. Snoeck, P. Fejes, P. Renaud and B. Chaudret, FeCo nanoparticles from an organometallic approach: synthesis, organisation and physical properties, *J. Mater. Chem.*, 2009, **19**, 3268.

14 C. Garnero, A. Pierrot, C. Gatel, C. Marcelot, R. Arenal, I. Florea, A. Bernard-Mantel, K. Soulantica, P. Poveda, B. Chaudret, T. Blon and L.-M. Lacroix, Single-crystalline body-centered FeCo nano-octopods: from one-pot chemical growth to a complex 3D magnetic configuration, *Nano Lett.*, 2021, **21**, 3664–3670.

15 L. A. Green, T. T. Thuy, D. Mott, S. Maenosono and N. T. Thanh, Multicore magnetic FePt nanoparticles: controlled formation and properties, *RSC Adv.*, 2014, **4**, 1039–1044.

16 Z. Meng, F. Xiao, Z. Wei, X. Guo, Y. Zhu, Y. Liu, G. Li, Z.-Q. Yu, M. Shao and W.-Y. Wong, Direct synthesis of L1o-FePt nanoparticles from single-source bimetallic complex and their electrocatalytic applications in oxygen reduction and hydrogen evolution reactions, *Nano Res.*, 2019, **12**, 2954–2959.

17 S. Mourdikoudis, V. Colliere, P. Fau and M. L. Kahn, A study on the synthesis of $Ni_{50}Co_{50}$ alloy nanostructures with tuned morphology through metal-organic chemical routes, *Dalton Trans.*, 2014, **43**, 8469–8479.

18 E. V. Gopalan, P. Joy, I. Al-Omari, D. S. Kumar, Y. Yoshida and M. Anantharaman, On the structural, magnetic and electrical properties of sol–gel derived nanosized cobalt ferrite, *J. Alloys Compd.*, 2009, **485**, 711–717.

19 E. Fantechi, C. Innocenti, M. Albino, E. Lottini and C. Sangregorio, Influence of cobalt doping on the hyperthermic efficiency of magnetite nanoparticles, *J. Magn. Magn. Mater.*, 2015, **380**, 365–371.

20 D. M. Clifford, C. E. Castano, A. J. Lu and E. E. Carpenter, Synthesis of FeCo alloy magnetically aligned linear chains by the polyol process: structural and magnetic characterization, *J. Mater. Chem. C*, 2015, **3**, 11029–11035.

21 R. Kappiyoor, M. Liangruksa, R. Ganguly and I. K. Puri, The effects of magnetic nanoparticle properties on magnetic fluid hyperthermia, *J. Appl. Phys.*, 2010, **108**, 094702.

22 G. Kandasamy and D. Maity, Recent advances in superparamagnetic iron oxide nanoparticles (SPIONs) for in vitro and in vivo cancer nanotheranostics, *Int. J. Pharm.*, 2015, **496**, 191–218.

23 A. H. Lu, E. L. Salabas and F. Schuth, Magnetic nanoparticles: synthesis, protection, functionalization, and application, *Angew. Chem., Int. Ed.*, 2007, **46**, 1222–1244.

24 Wahajuddin and S. Arora, Superparamagnetic iron oxide nanoparticles: magnetic nanoplatforms as drug carriers, *Int. J. Nanomed.*, 2012, **7**, 3445–3471.

25 W. Wu, Z. Wu, T. Yu, C. Jiang and W. S. Kim, Recent progress on magnetic iron oxide nanoparticles: synthesis, surface functional strategies and biomedical applications, *Sci. Technol. Adv. Mater.*, 2015, **16**, 023501.

26 L. Wu, A. Mendoza-Garcia, Q. Li and S. Sun, Organic Phase Syntheses of Magnetic Nanoparticles and Their Applications, *Chem. Rev.*, 2016, **116**, 10473–10512.

27 M. Unni, A. M. Uhl, S. Savliwala, B. H. Savitzky, R. Dhavalikar, N. Garraud, D. P. Arnold, L. F. Kourkoutis,

J. S. Andrew and C. Rinaldi, Thermal decomposition synthesis of iron oxide nanoparticles with diminished magnetic dead layer by controlled addition of oxygen, *ACS Nano*, 2017, **11**, 2284–2303.

28 B. Kandapallil, B. R. E. Colborn, P. J. Bonitatibus and F. Johnson, Synthesis of high magnetization Fe and FeCo nanoparticles by high temperature chemical reduction, *J. Magn. Magn. Mater.*, 2015, **378**, 535–538.

29 A. N. Popova, Synthesis and Characterization of Iron-Cobalt Nanoparticles, *J. Phys.: Conf. Ser.*, 2012, **345**, 012030.

30 C. Desvaux, C. Amiens, P. Fejes, P. Renaud, M. Respaud, P. Lecante, E. Snoeck and B. Chaudret, Multimillimetre-large superlattices of air-stable iron-cobalt nanoparticles, *Nat. Mater.*, 2005, **4**, 750–753.

31 C. Desvaux, P. Lecante, M. Respaud and B. Chaudret, Structural and magnetic study of the annealing of Fe-Co nanoparticles, *J. Mater. Chem.*, 2010, **20**, 103–109.

32 I. Robinson, S. Zacchini, L. D. Tung, S. Maenosono and N. T. K. Thanh, Synthesis and Characterization of Magnetic Nanoalloys from Bimetallic Carbonyl Clusters, *Chem. Mater.*, 2009, **21**, 3021–3026.

33 C. Wang, S. Peng, L.-M. Lacroix and S. Sun, Synthesis of high magnetic moment CoFe nanoparticles via interfacial diffusion in core/shell structured Co/Fe nanoparticles, *Nano Res.*, 2010, **2**, 380–385.

34 J. Park, K. An, Y. Hwang, J. G. Park, H. J. Noh, J. Y. Kim, J. H. Park, N. M. Hwang and T. Hyeon, Ultra-large-scale syntheses of monodisperse nanocrystals, *Nat. Mater.*, 2004, **3**, 891–895.

35 K. An, N. Lee, J. Park, S. C. Kim, Y. Hwang, J.-G. Park, J.-Y. Kim, J.-H. Park, M. J. Han, J. Yu and T. Hyeon, Synthesis, Characterization, and Self-Assembly of Pencil-Shaped CoO Nanorods, *J. Am. Chem. Soc.*, 2006, **128**, 9753–9760.

36 L. Storozhuk, M. O. Besenhard, S. Mourdikoudis, A. P. LaGrow, M. R. Lees, L. D. Tung, A. Gavriilidis and N. T. K. Thanh, Stable Iron Oxide Nanoflowers with Exceptional Magnetic Heating Efficiency: Simple and Fast Polyol Synthesis, *ACS Appl. Mater. Interfaces*, 2021, **13**, 45870–45880.

37 J. V. Hoene, R. G. Charles and W. M. Hickam, Thermal Decomposition of Metal Acetylacetonates: Mass Spectrometer Studies, *J. Phys. Chem.*, 1958, **62**, 1098–1101.

38 S. Ramanavicius, R. Zalneravicius, G. Niaura, A. Drabavicius and A. Jagminas, Shell-dependent antimicrobial efficiency of cobalt-ferrite nanoparticles, *Nano-Struct. Nano-Objects*, 2018, **15**, 40–47.

39 M. Houshiar, F. Zebhi, Z. J. Razi, A. Alidoust and Z. Askari, Synthesis of cobalt ferrite ($CoFe_2O_4$) nanoparticles using combustion, coprecipitation, and precipitation methods: A comparison study of size, structural, and magnetic properties, *J. Magn. Magn. Mater.*, 2014, **371**, 43–48.

40 I. Malinowska, Z. Ryzynska, E. Mrotek, T. Klimczuk and A. Zielinska-Jurek, Synthesis of $CoFe_2O_4$ nanoparticles: The effect of ionic strength, concentration, and precursor type on morphology and magnetic properties, *J. Nanomater.*, 2020, **2020**, 9046219.

41 H. Kennaz, A. Harat, O. Guellati, D. Y. Momodu, F. Barzegar, J. K. Dangbegnon, N. Manyala and M. Guerioune, Synthesis and electrochemical investigation of spinel ferrite magnetic nanoparticles for supercapacitor application, *J. Solid State Electrochem.*, 2018, **22**, 835–847.

42 K. Sinko, E. Manek, A. Meiszterics, K. Havancsak, U. Vainio and H. Peterlik, Liquid-phase syntheses of cobalt ferrite nanoparticles, *J. Nanopart. Res.*, 2012, **14**, 894.

43 K. Henry, J. K. Ahlburg, H. L. Andersen, C. Granados-Miralles, M. Stingaciu, M. Saura-Muzquiz and M. Christensen, In-depth investigations of size and occupancies in cobalt ferrite nanoparticles by joint Rietveld refinements of X-ray and neutron powder diffraction data, *J. Appl. Crystallogr.*, 2022, **55**, 1336–1350.

44 W. Baaziz, B. P. Pichon, Y. Liu, J.-M. Greneche, C. Ulhaq-Bouillet, E. Terrier, N. Bergeard, V. Halte, C. Boeglin, F. Choueikani, M. Toumi, T. Mhiri and S. Begin-Colin, Tuning of synthesis conditions by thermal decomposition toward core-shell $Co_xFe_{1(-x}O@Co_yFe_{3(-y)}O_4$ and $CoFe_2O_4$ nanoparticles with spherical and cubic shapes, *Chem. Mater.*, 2014, **26**, 5063.

45 N. Poudyal, G. S. Chaubey, C. B. Rong, J. Cui and J. P. Liu, Synthesis of monodisperse FeCo nanoparticles by reductive salt-matrix annealing, *Nanotechnology*, 2013, **24**, 345605.

46 G. S. Chaubey, C. Barcena, N. Poudyal, C. Rong, J. Gao, S. Sun and J. P. Liu, Synthesis and stabilization of FeCo nanoparticles, *J. Am. Chem. Soc.*, 2007, **129**, 7214–7215.

47 Z. Yan, S. FitzGerald, T. M. Crawford and O. Thompson, Mefford. Oxidation of wustite rich iron oxide nanoparticles via post-synthesis annealing, *J. Magn. Magn. Mater.*, 2021, **539**, 168405.

48 L. Lartigue, P. Hugounenq, D. Alloyeau, S. P. Clarke, M. Levy, J. C. Bacri, R. Bazzi, D. F. Brougham, C. Wilhelm and F. Gazeau, Cooperative organization in iron oxide multi-core nanoparticles potentiates their efficiency as heating mediators and MRI contrast agents, *ACS Nano*, 2012, **6**, 10935–10949.

49 P. Hugounenq, M. Levy, D. Alloyeau, L. Lartigue, E. Dubois, V. Cabuil, C. Ricolleau, S. Roux, C. Wilhelm, F. Gazeau and R. Bazzi, Iron Oxide Monocrystalline Nanoflowers for Highly Efficient Magnetic Hyperthermia, *J. Phys. Chem. C*, 2012, **116**, 15702–15712.

50 C. Blanco-Andujar, D. Ortega, P. Southern, Q. A. Pankhurst and N. T. K. Thanh, High performance multi-core iron oxide nanoparticles for magnetic hyperthermia: microwave synthesis, and the role of core-to-core interactions, *Nanoscale*, 2015, **7**, 1768–1775.

51 C. Cannas, A. Musinu, D. Peddis and G. Piccaluga, Synthesis and characterization of $CoFe_2O_4$ nanoparticles dispersed in a silica matrix by a sol-gel autocombustion method, *Chem. Mater.*, 2006, **18**, 3835–3842.

52 L. A. Garcia Cerda and S. M. Montemayor, Synthesis of $CoFe_2O_4$ nanoparticles embedded in a silica matrix by the citrate precursor technique, *J. Magn. Magn. Mater.*, 2005, **294**, e43–e46.

53 F. J. Yang, J. Yao, J. J. Min, J. H. Li and X. Q. Chen, Synthesis of high saturation magnetization FeCo nano-

particles by polyol reduction method, *Chem. Phys. Lett.*, 2016, **648**, 143–146.

54 D. Kodama, K. Shinoda, K. Sato, Y. Konno, R. J. Joseyphus, K. Motomiya, H. Takahashi, T. Matsumoto, Y. Sato, K. Tohji and B. Jeyadevan, Chemical Synthesis of Sub-micrometer- to Nanometer-Sized Magnetic FeCo Dice, *Adv. Mater.*, 2006, **18**, 3154–3159.

55 M. Zamanpour, Y. Chen, B. Hu, K. Carroll, Z. J. Huba, E. E. Carpenter, L. H. Lewis and V. G. Harris, Large-scale synthesis of high moment FeCo nanoparticles using modified polyol synthesis, *J. Appl. Phys.*, 2012, **111**, 07B528.

56 T. Q. Huy, P. Van Chung, N. T. Thuy, C. Blanco-Adujar and N. T. K. Thanh, Protein A-conjugated iron oxide nanoparticles for separation of Vibrio cholerae from water samples, *Faraday Discuss.*, 2014, **175**, 73–82.

57 N. A. Frey, S. Peng, K. Cheng and S. Sun, Magnetic nanoparticles: synthesis, functionalization, and applications in bioimaging and magnetic energy storage, *Chem. Soc. Rev.*, 2009, **38**, 2532–2542.

58 G. Reiss and A. Hutten, Magnetic nanoparticles: applications beyond data storage, *Nat. Mater.*, 2005, **4**, 725–726.

59 D. Tomar and P. Jeevanandam, Synthesis of cobalt ferrite nanoparticles with different morphologies via thermal decomposition approach and studies on their magnetic properties, *J. Alloys Compd.*, 2020, **843**, 155815.

60 D. Tomar and P. Jeevanandam, Synthesis of $CoFe_2O_4$ nanoparticles via thermal decomposition of Co-Fe bimetallic glycolates: effect of using different cobalt precursors on their morphology and magnetic properties, *J. Supercond. Novel Magn.*, 2023, **36**, 1717.

61 S. Shanmugam and B. Subramanian, Evolution of phase pure magnetic cobalt ferrite nanoparticles by varying the synthesis conditions of polyol method, *Mater. Sci. Eng. B*, 2020, **252**, 114451.

62 L. V. Leonel, J. B. S. Barbosa, D. R. Miquita, F. P. Oliveira, L. E. Fernandez-Outon, E. F. Oliveira and J. D. Ardisson, Facile polyol synthesis of ultrasmall water-soluble cobalt ferrite nanoparticles, *Solid State Sci.*, 2018, **86**, 45–52.

63 D. Kodama, K. Shinoda, K. Sato, Y. Sato, B. Jeyadevan and K. Tohji, Synthesis of Fe-Co alloy particles by modified polyol process, *IEEE Trans. Magn.*, 2006, **42**, 2796–2798.

64 D. Yi, B. Chaudret and K. Soulantica, Chapter 5: Gases, in *Reducing agents in colloidal nanoparticle synthesis*, ed. S. Mourdikoudis, The Royal Society of Chemistry, 2021. DOI: **10.1039/9781839163623-00097**.

65 N. Nitin, L. E. W. LaConte, O. Zurkiya, X. Hu and G. Bao, Functionalization and peptide-based delivery of magnetic nanoparticles as an intracellular MRI contrast agent, *J. Biol. Inorg. Chem.*, 2004, **9**, 706–712.

66 R. Wang, R. Xiao, Z. Zeng, L. Xu and J. Wang, Application of poly(ethylene glycol)-distearoylphosphatidylethanolamine (PEG-DSPE) block copolymers and their derivatives as nanomaterials in drug delivery, *Int. J. Nanomed.*, 2012, **7**, 4185–4198.

67 J. Marbaix, N. Mille, L.-M. Lacroix, J. M. Asensio, P.-F. Fazzini, K. Soulantica, J. Carrey and B. Chaudret, Tuning the composition of FeCo nanoparticle heating agents for magnetically induced catalysis, *ACS Appl. Nano Mater.*, 2020, **3**, 3767–3778.

68 M. Angelakeris, Chapter 11 Magnetic particle hyperthermia, in *21st Century Nanoscience–A Handbook*, ed. K. D. Sattler, CRC Press, 2020.

69 L.-M. Lacroix, R. Bel Malaki, J. Carrey, S. Lachaize, M. Respaud, E. Snoeck and B. Chaudret, Magnetic hyperthermia in single-domain monodisperse FeCo nanoparticles: Evidences for Stoner–Wohlfarth behavior and large losses, *J. Appl. Phys.*, 2009, **105**, 023911.

70 O. M. Lemine, S. Algessair, N. Madkhali, B. Al-Najar and K. El-Boubbou, Assessing the heat generation and self-heating mechanism of superparamagnetic Fe_3O_4 nanoparticles for magnetic hyperthermia application: the effects of concentration, frequency, and magnetic field, *Nanomaterials*, 2023, **13**, 453.